AD-A087 397 ORINCON CORP LA JOLLA CA F/G 12/1
INTERNAL WAVE MEASUREMENTS FOR STATISTICAL HYPOTHESIS TESTING.(U)
MAY 80 R A ALTES N00014-79-C-0948
UNCLASSIFIED OC-R-80-0948-2 NL

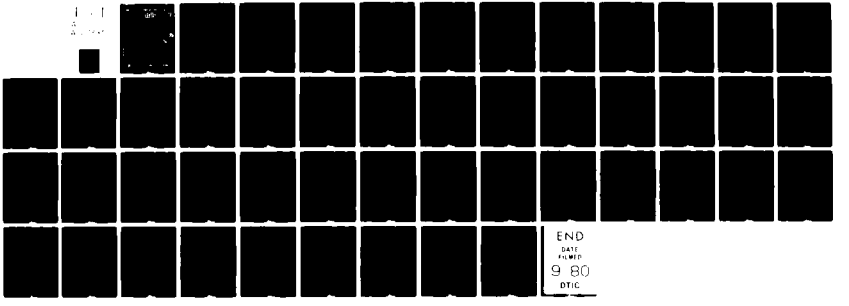

END
DATE FILMED
9 80
DTIC

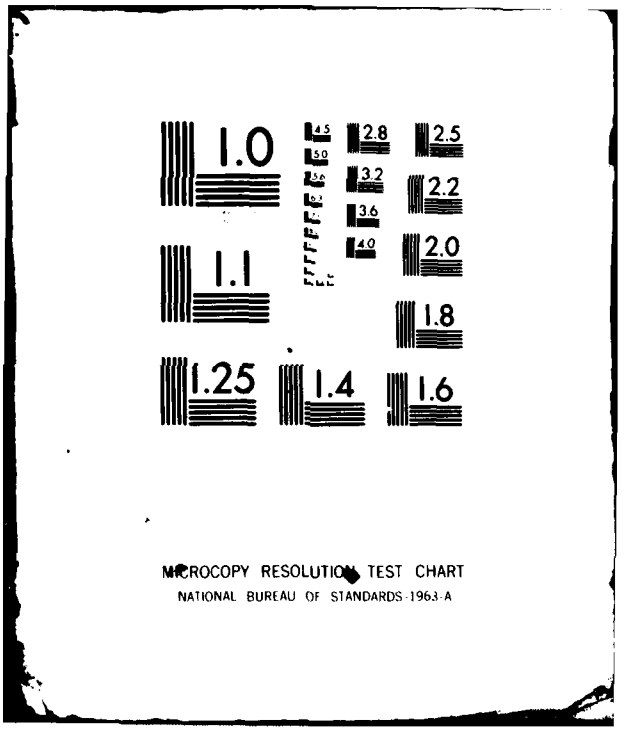
1.0
1.1
1.25
1.4
1.6
1.8
2.0
2.2
2.5
2.8
3.2
3.6
4.0
4.5
5.0
MICROCOPY RESOLUTION TEST CHART
NATIONAL BUREAU OF STANDARDS-1963-A

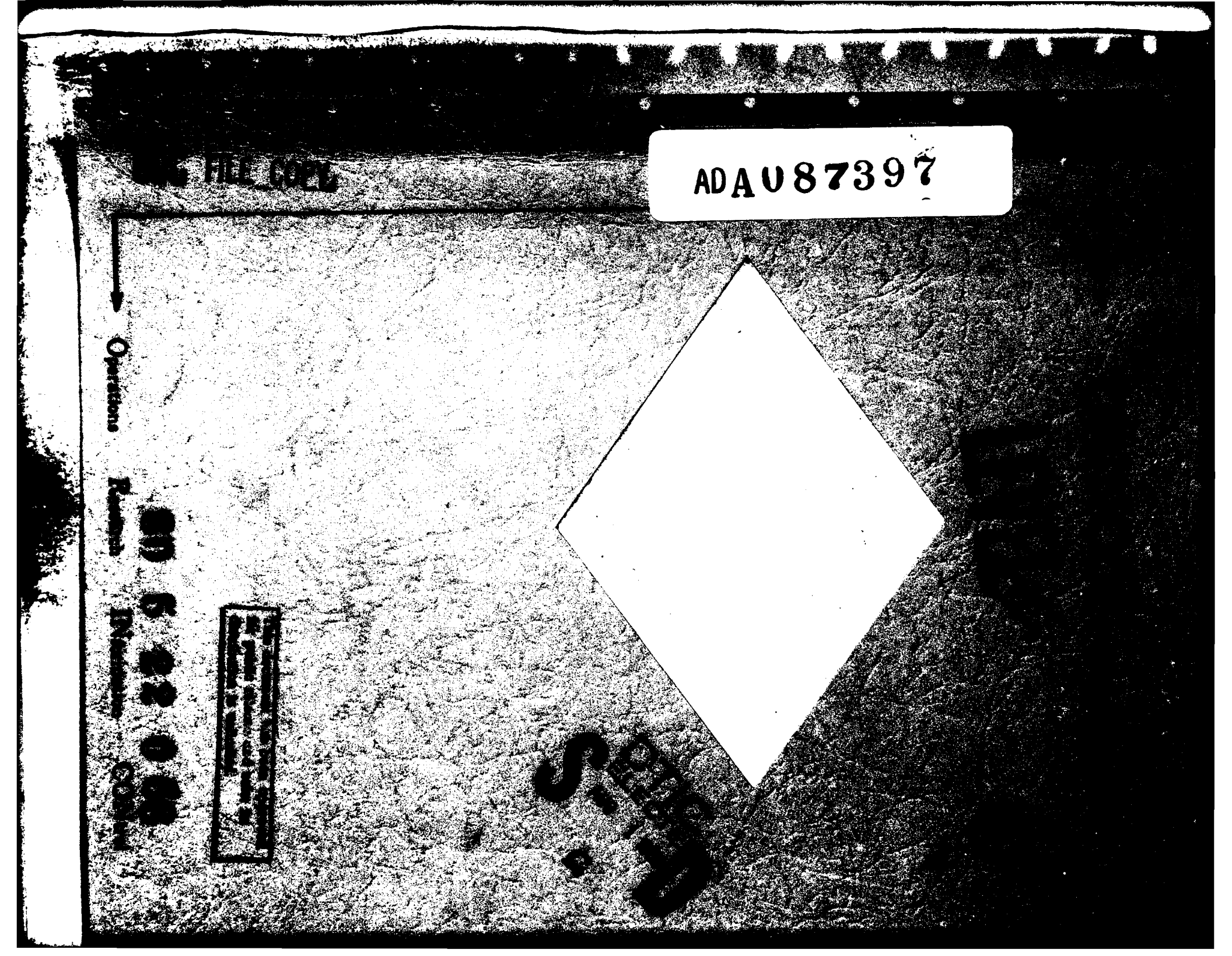
AD A087397
Operations
Research

ORINCON Corporation

3366 No. Torrey Pines Ct., Suite 320, La Jolla, CA 92037 (714) 455-5530

(14) OC-R-80-0948-2

(11) 5 May 1980

(12) 149

(11)

(6) INTERNAL WAVE MEASUREMENTS FOR STATISTICAL HYPOTHESIS TESTING

(9) Final Report

Contract No. N00014-79-C-0948

(15)

Prepared by: Richard A. Altes

(10) Richard A. Altes
Principal Investigator

Approved by: John T. Rickard

John T. Rickard
Program Manager

Submitted to: Mr. Mike Stanley
Code 500
NORDA
Bay St. Louis, Miss. 39529

Operations Research INformation CONtrol

10

TABLE OF CONTENTS

TABLE OF CONTENTS (CONCLUDED)

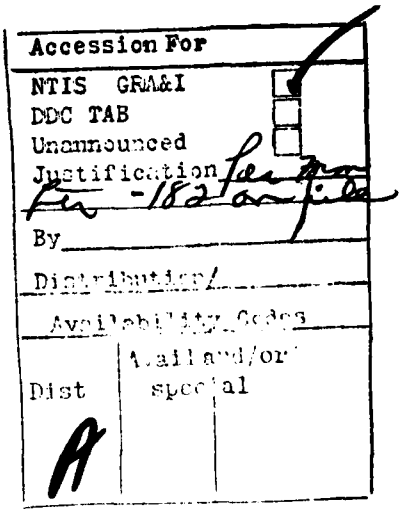

ORINCON

1.0 ABSTRACT

If internal wave measurements are to be used for a hypothesis test, then the best description of the measurements is a multivariate probability density function. This report discusses the estimation of such a probability distribution, along with the associated concepts of Gaussianity, stationarity, homogeneity, isotropy, and frequency-wave number spectra for random fields. By drawing upon these concepts, the report offers suggestions for thermistor or current meter placement, for Doppler sonar design, and for tests of Gaussianity and stationarity.

2.0 INTRODUCTION

Internal waves can be described in many different ways. The description that is most useful to a detection theorist is a statistical one. A detector is designed to test two hypotheses, H_1 vs. H_0. Under H_1, data consists of a signal (an unnatural disturbance of the internal wave environment), along with naturally-occurring internal waves and noise. Under H_0, data consists of measurements of a natural internal wave environment, along with noise that is introduced by the measurement system. In summary

$$\begin{aligned} H_1&: \text{ Signal + natural background + noise} \\ H_0&: \text{ Natural background + noise.} \end{aligned} \tag{1}$$

In order to distinguish between H_1 and H_0, one can assign costs to correct and incorrect judgements, and try to minimize the expected risk. Alternatively, one can fix the probability of a false alarm (saying that H_1 is true when, in fact, H_0 is true) and find a test that maximizes the probability of detection (correctly stating that H_1 is true). In either case, the resulting hypothesis test is implemented by forming a likelihood ratio [1]

$$\frac{p(\text{data}\,|\,H_1)}{p(\text{data}\,|\,H_0)} \underset{H_0}{\overset{H_1}{\gtrless}} \text{Threshold} = \gamma \tag{2}$$

where

$$p(\text{data}\,|\,H_i) = \text{the probability that the measured data would be observed if } H_i \text{ were true, } i = 1 \text{ or } 0. \tag{3}$$

The double inequality in (1) means the detector says that H_1 is true if $p(\text{data}|H_1) \geq \gamma\, p(\text{data}|H_0)$, and the detector decides that H_0 is true otherwise.

From the viewpoint of a statistical hypothesis test, one can say that the internal wave background is specified when $p(\text{data}|H_0)$ is known. "Environmental characterization" is then equivalent to finding $p(\text{data}|H_0)$, for any given sensor array. A complete description of the environment implies that the data is measured in such a way that no extra information would be obtained if additional sensors were used.

This report is concerned with measurement methods and signal processing ideas that can be used to obtain a complete specification of the internal wave background, in the sense that $p(\text{data}|H_0)$ is estimated, and no additional sensors will change this estimate (except to decrease measurement errors).

3.0 SAMPLING INTERVALS AND STATIONARITY

3.1 Sampling Intervals

Given sampled data descriptions over a given interval of time and space, the number of data samples depends upon the sampling rate. The minimum sampling rate that is required to completely specify a given function is equal to twice the bandwidth of the function [2].

The temporal bandwidth of internal waves is approximately 3×10^{-3} Hz [3], so time samples from any given sensor should be separated by less than 160 sec, i.e.,

$$\text{Temporal sampling rate} \geq 2\,B_t \approx 6 \times 10^{-3}\ \text{Hz} \tag{4}$$

$$\text{Sampling interval} \leq (2\,B_t)^{-1} \approx 160\ \text{sec.} \tag{5}$$

The spatial bandwidth can be determined from wavelength, λ. In the horizontal plane [4, 5]

$$20\ \text{m} < \lambda < 1000\ \text{m.}$$

For vertically propagating internal wave components, the same range of wavelengths is found [6]. Thus, for both horizontal and vertical directions,

$$.05\ \text{m}^{-1} > k/2\pi > .001\ \text{m}^{-1} \tag{6}$$

$$\text{Spatial sampling rate} \geq 2 \times .05\ \text{m}^{-1} \tag{7}$$

$$\text{Sampling interval} \leq 10\ \text{m.} \tag{8}$$

Equation (8) implies that the internal wave environment should be sampled at 10 m intervals (or less), in both the horizontal and vertical directions. At each spatial sampling point, time samples should be obtained at least every 160 sec.

3.2 Stationarity Assumptions

For any large volume of ocean, the foregoing analysis seems to necessitate the use of three dimensional arrays of sensors that fill the whole volume, with sensors 10 m apart. Even with Doppler sonars, which can remotely measure velocity at a given point, we apparently need sonar beams that point in all directions, in order to achieve the required sampling density in azimuth and elevation. Furthermore, it is difficult to envision any simple way to estimate $p(\text{data}\,|\,H_0)$, if the joint probability of any two measurements depends upon the times at which the measurements are taken (rather than the difference in times).

If it can be assumed that the data is spatially and temporally stationary, then the problems of dimensionality and sampling are considerably reduced.

3.2.1 Stationarity in Time

Stationarity in time implies that $p(\text{data}\,|\,H_0)$ does not depend upon the particular time interval over which the data is measured. This assumption, together with ergodicity, allows an observer to estimate $p(\text{data}\,|\,H_0)$ by the usual histogram approach, or by use of Parzen windows [7, 8] or moment estimates [9, 10].

The dimensionality of the observation space is still very large, even with a stationarity assumption. Suppose that we measure the responses of N different spatially distributed sensors at

times t_1, t_2, ..., t_M. There are M possible time differences in this sequence, ranging from $t_1 - t_1$ to $t_M - t_1$. For each time difference, there are N different components of the data. The dimensionality of the observation space is then N x M. For pdf estimation,* the number of sample values should be much larger than the dimensionality of the observation space.

3.2.2 Spatial Stationarity

3.2.2.1 Homogeneity and Isotropy

Two kinds of spatial stationarity can be defined [11]. Given a point $\underline{x} = x_1, x_2, x_3$ in a three dimensional space, we measure a random function $a(\underline{x})$ at this point. The random functions $a(\underline{x})$ for various $\underline{x}$-values or positions in the space form samples of a random field.

The most general version of wide-sense stationarity for such a set of random functions is to assume that $a(\underline{x})$ is homogeneous. For a homogeneous random field [11],

$$E\{a(\underline{x})\} = 0 \tag{9}$$

$$E\{a(\underline{x})a^*(\underline{x}')\} = R(\underline{x}' - \underline{x}). \tag{10}$$

The covariance between the random functions that are measured at different points in the field then depends only on the magnitude and direction of the vector that separates these points.

---

*"pdf" stands for "probability density function."

A less general version of spatial stationarity is a random field that is both homogeneous and isotropic. For a homogeneous, isotropic random field,

$$E\{a(\underline{x})\} = 0$$

$$E\{a(\underline{x})\, a^*(\underline{x}')\} = R(\|\underline{x}' - \underline{x}\|), \tag{11}$$

where $\|\underline{x}' - \underline{x}\|$ is the magnitude of the vector that separates $\underline{x}'$ and $\underline{x}$. An isotropic random field thus exhibits no direction dependence, and the covariance between random functions measured at different locations depends only on the distance between these locations.

Both homogeneous and homogeneous-isotropic random fields have spectral distribution functions and corresponding spectral density functions. If the field is not isotropic, the spectral density function depends upon a vector wave number $\underline{k}$:

$$S(k_1, k_2, k_2, \omega) = \iiiint_{-\infty}^{\infty} R(\Delta x_1, \Delta x_2, \Delta x_3, \Delta t)\, e^{-j(k_1 \Delta x_1 + k_2 \Delta x_2 + k_3 \Delta x_3 + \omega \Delta t)}\, d(\Delta x_1)\, d(\Delta x_2)\, d(\Delta x_3)\, d(\Delta t), \tag{12}$$

where $\underline{x}' - \underline{x}$ has components $(\Delta x_1, \Delta x_2, \Delta x_3)$.

For a homogeneous-isotropic random field

$$S(k, \omega) = \iint_{-\infty}^{\infty} R(\Delta x, \Delta t)\, e^{-j(k\Delta x + \omega \Delta t)}\, d(\Delta x)\, d(\Delta t) \tag{13}$$

where

$$\|\underline{x}' - \underline{x}\| = \Delta x. \tag{14}$$

3.2.2.2 Implications and Applicability of Homogeneity and Isotropy

If the data were both homogeneous and isotropic, there would be a significant reduction in the required number of sensors or Doppler sonar beams. A single beam or a line of sensors would be sufficient to generate the frequency-wave number spectrum in (13).

The ocean, however, is not physically isotropic in three dimensions. In fact, the ocean is not even homogeneous in the vertical direction, since many physical constants change with pressure and salinity (not to mention the effect of surface and bottom). A homogeneous-isotropic assumption in three dimensions is thus blatantly unrealistic, unless it is made with respect to a limited depth interval. Homogeneity within such a limited interval would correspond to the concept of local stationarity [12].

Although it is physically unreasonable to assume that homogeneity exists in the vertical direction, it would seem that both homogeneity and isotropy should apply in the horizontal plane, at any given depth. This observation implies that

$$E\{a(\underline{x})a^*(\underline{x}')\} = R(\Delta x_{12}, x_3, x_3'). \tag{15}$$

In a horizontal plane at depth x_3, where

$$x_3' - x_3 \equiv 0 \tag{16}$$

we have

$$S_{x_3}(k, \omega) = \iint_{-\infty}^{\infty} R(\Delta x_{12}, x_3, x_3, \Delta t) \, e^{-j(k \Delta x_{12} + \omega \Delta t)} \, d(\Delta x_{12}) \, d(\Delta t). \quad (17)$$

Equation (17) implies that we expect to see different frequency-wave number spectra in horizontal planes at different depths, because of the vertical inhomogeneity of the ocean.

From our sampling results, $S_{x3}(k, \omega)$ should be measured at depths that are less than ten meters apart. If a Doppler sonar beam is tilted in such a way as to measure internal wave velocity at a range of depths that exceeds 10 m, then we must be careful in our interpretation of the results. Unless it is assumed that local stationarity exists within the depth range that is sampled, the data must be segmented into 10 m depth intervals, and only the data from each interval is then used to estimate $S_{x_3}(k, \omega)$. Given this analysis procedure, a single beam of a Doppler sonar or a single line array is sufficient to estimate $R(\Delta x_{12}, x_3, x_3)$.

The assumption of horizontal isotropy can be checked by measuring the internal wave field along orthogonal directions in a given horizontal plane. If

$$R(\Delta x_1, 0, x_3, x_3) \neq R(0, \Delta x_2, x_3, x_3) \quad (18)$$

then the process is not isotropic. In this case, we have

$$S_{x_3}(k_1, k_2, \omega) = \iiint_{-\infty} R(\Delta x_1, \Delta x_2, x_3, x_3, \Delta t) \, e^{-j(k_1 \Delta x_1 + k_2 \Delta x_2 + \omega \Delta t)} \, d(\Delta x_1) \, d(\Delta x_2) \, d(\Delta t). \quad (19)$$

For a homogeneous, non-isotropic wave field, measurements become much more difficult. In general, it is impossible to measure $R(\Delta x_1, \Delta x_2, x_3, x_3)$ with two orthogonal sonar beams or line arrays, since $R(0, \Delta x_2, x_3, x_3)$ and $R(\Delta x_1, 0, x_3, x_3)$ do not completely describe the autocovariance function of the data. For homogeneous, non-isotropic wave fields, a further simplifying assumption is needed for convenient data gathering.

3.2.2.3 Separability for Homogeneous, Non-Isotropic Random Fields

The most obvious simplifying assumption for the analysis of homogeneous, non-isotropic fields is separability of the autocovariance function. By separability, we mean that

$$R(\Delta x_1, \Delta x_2, x_3, x_3, \Delta t) = R^{(1)}(\Delta x_1, 0, x_3, x_3, \Delta t) \cdot R^{(2)}(0, \Delta x_2, x_3, x_3, \Delta t). \quad (20)$$

For example, if

$$R(\Delta x_1, \Delta x_2) = \sum_{m,n} c_{mn} \cos\left(\frac{2\pi m \Delta x_1}{T}\right) \cos\left(\frac{2\pi n \Delta x_2}{T}\right), \quad (21)$$

then $R(\Delta x_1, \Delta x_2)$ is separable if

$$c_{mn} = a_m b_n. \tag{22}$$

In general, (20) implies that

$$S_{x_3}(k_1, k_2, \omega) = S^{(1)}_{x_3}(k_1, \omega)\, S^{(2)}_{x_3}(k_2, \omega). \tag{23}$$

From (20), separability implies that the random field can be completely described by measurements along two orthogonal directions, using two orthogonal sonar beams or line arrays. This measurement scenario is much simpler than full two dimensional sampling.

If we plan to invoke a separability assumption, then we should check this assumption by measuring data along a third direction or at a point outside the two original lines. Is the covariance at this point, relative to a point at the origin, given by the product of two other covariance functions, as in (20)?

3.2.2.4 Applicability of the Separability Assumption

Physically, it would seem that separability will occur infrequently in situations where there is a preferred direction of wave propagation. Consider the observation of wind-propagated surface waves that are all moving in the same direction. The resulting field may be homogeneous, but it is not isotropic. If the waves are observed with one axis pointing into the wind and the other orthogonal to the direction of propagation, then the covariance of the wave field probably can be described by a separable function. If,

however, the axes are pointing in any other direction, then the measured autocovariance function will not be separable. Separability is thus orientation-dependent.

In situations where there is no preferred direction of propagation, separability may be a reasonable assumption. If a check shows that the data is non-separable, then a rotation of coordinates may rectify the situation.

4.0 GAUSSIANITY

4.1 Implications of Gaussianity

Homogeneous random fields and frequency-wave number spectra are basic to second-order characterizations of internal wave measurements. If all the data samples are individually and jointly Gaussian, then second-order characterizations are sufficient to completely describe the process.

4.2 A Test for Multivariate Joint Gaussianity

We are given a sequence of measurements $\underline{a}(t_1)$, $\underline{a}(t_2)$, ..., $\underline{a}(t_M)$ from N sensors at various positions in the wave field, or from different resolution cells of a Doppler sonar. We assume that $t_n - t_{n-1} \gg 160$ sec, so the samples are statistically independent. At time t_1, for example,

$$\underline{a}(t_1) = [a_1(t_1)\ a_2(t_1)\ \ldots\ a_N(t_1)]^T \tag{24}$$

where $a_1(t_1)$ is the measurement from the first sensor at time t_1.

4.2.1 The Standard Chi-Square Test

To determine whether $\{a_1(t_m)\}_{m=1}^{M}$ is individually Gaussian, we can divide the observed range of a_1-values into I intervals, such that there are at least ten samples in each interval. The mean and variance of $\{a_1(t_m)\}_{m=1}^{M}$ are measured, and the corresponding Gaussian distribution $p(a_1)$ is constructed. The area of the Gaussian distribution that is contained in each of the I intervals is determined. The resulting areas are denoted p_i, and they are the probability that

a Gaussian-distributed data point will fall within the i^{th} interval. For M data points, we expect Mp_i points to fall within the i^{th} interval if the random variable a_1 is Gaussian. In fact, ν_i data points are found to fall within the i^{th} interval, where we have constructed the interval size such that $\nu_i > 10$.

A standard chi-square test with I-1 degrees of freedom can now be applied [13]. Let

$$\chi^2 = \sum_{i=1}^{I} \frac{(\nu_i - Mp_i)^2}{Mp_i}. \tag{25}$$

The hypothesis that the observed data is Gaussian is rejected if

$$\chi^2 > \chi_p^2. \tag{26}$$

If the observed data from the first sensor really is Gaussian, then the probability that $\chi^2 > \chi_p^2$ is p%, which is the level of significance of the test. From Table 1 [13, 14], if I = 5 and the level of significance is 5%, we say that the data is non-Gaussian only if $\chi^2 > 9.488$.

4.2.2 A Modified Chi-Square Test for Multivariate Data

For multivariate data, N sensors or resolution cells form an N-dimensional observation space, and the set of measurements $\underline{a}(t_1)$ defines a sample point in the space. The independent measurements $\{\underline{a}(t_m)\}_{m=1}^{M}$ yield M such sample points.

The sample mean and covariance matrix are

$$\underline{\mu} = \frac{1}{M} \sum_{m=1}^{M} \underline{a}(t_m) \tag{27}$$

Table 1.

The χ^2-Distribution [13, 14]

Let $p_n(x)$ be the p. d. f., the χ^2-distribution with n degrees of freedom. The p percent value χ^2_p of χ^2 for n d. of fr. is a value such that the probability that an observed value of χ^2 exceeds χ^2_p is

$$P = \frac{p}{100} = P(\chi^2 > \chi^2_p) = \int_{\chi^2_p}^{\infty} p_n(x)\,dx.$$

Degrees of freedom n	χ^2_p as a function of n and $p = 100P$													
	p=99	98	95	90	80	70	50	30	20	10	5	2	1	0.1
1	0.000	0.001	0.004	0.016	0.064	0.148	0.455	1.074	1.642	2.706	3.841	5.412	6.635	10.827
2	0.020	0.040	0.103	0.211	0.446	0.713	1.386	2.408	3.219	4.605	5.991	7.824	9.210	13.815
3	0.115	0.185	0.352	0.584	1.005	1.424	2.366	3.665	4.642	6.251	7.815	9.837	11.341	16.266
4	0.297	0.429	0.711	1.064	1.649	2.195	3.357	4.878	5.989	7.779	9.488	11.668	13.277	18.466
5	0.554	0.752	1.145	1.610	2.343	3.000	4.351	6.064	7.289	9.236	11.070	13.388	15.086	20.517
6	0.872	1.134	1.635	2.204	3.070	3.828	5.348	7.231	8.558	10.645	12.592	15.033	16.812	22.457
7	1.239	1.564	2.167	2.833	3.822	4.671	6.346	8.383	9.803	12.017	14.067	16.622	18.475	24.322
8	1.646	2.032	2.733	3.490	4.594	5.527	7.344	9.524	11.030	13.362	15.507	18.168	20.090	26.125
9	2.088	2.532	3.325	4.168	5.380	6.393	8.343	10.656	12.242	14.684	16.919	19.679	21.666	27.877
10	2.558	3.059	3.940	4.865	6.179	7.267	9.342	11.781	13.442	15.987	18.307	21.161	23.209	29.588
11	3.053	3.609	4.575	5.578	6.989	8.148	10.341	12.899	14.631	17.275	19.675	22.618	24.725	31.264
12	3.571	4.178	5.226	6.304	7.807	9.034	11.340	14.011	15.812	18.549	21.026	24.054	26.217	32.909
13	4.107	4.765	5.892	7.042	8.634	9.926	12.340	15.119	16.985	19.812	22.362	25.472	27.688	34.528
14	4.660	5.368	6.571	7.790	9.467	10.821	13.339	16.222	18.151	21.064	23.685	26.873	29.141	36.123
15	5.229	5.985	7.261	8.547	10.307	11.721	14.339	17.322	19.311	22.307	24.996	28.259	30.578	37.697
16	5.812	6.614	7.962	9.312	11.152	12.624	15.338	18.418	20.465	23.542	26.296	29.633	32.000	39.252
17	6.408	7.255	8.672	10.085	12.002	13.531	16.338	19.511	21.615	24.769	27.587	30.995	33.409	40.790
18	7.015	7.906	9.390	10.865	12.857	14.440	17.338	20.601	22.760	25.989	28.869	32.346	34.805	42.312
19	7.633	8.567	10.117	11.651	13.716	15.352	18.338	21.689	23.900	27.204	30.144	33.687	36.191	43.820
20	8.260	9.237	10.851	12.443	14.578	16.266	19.337	22.775	25.038	28.412	31.410	35.020	37.566	45.315
21	8.897	9.915	11.591	13.240	15.445	17.182	20.337	23.858	26.171	29.615	32.671	36.343	38.932	46.797
22	9.542	10.600	12.338	14.041	16.314	18.101	21.337	24.939	27.301	30.813	33.924	37.659	40.289	48.268
23	10.196	11.293	13.091	14.848	17.187	19.021	22.337	26.018	28.429	32.007	35.172	38.968	41.638	49.728
24	10.856	11.992	13.848	15.659	18.062	19.943	23.337	27.096	29.553	33.196	36.415	40.270	42.980	51.179
25	11.524	12.697	14.611	16.473	18.940	20.867	24.337	28.172	30.675	34.382	37.652	41.566	44.314	52.620
26	12.198	13.409	15.379	17.292	19.820	21.792	25.336	29.246	31.795	35.563	38.885	42.856	45.642	54.052
27	12.879	14.125	16.151	18.114	20.703	22.719	26.336	30.319	32.912	36.741	40.113	44.140	46.963	55.476
28	13.565	14.847	16.928	18.939	21.588	23.647	27.336	31.391	34.027	37.916	41.337	45.419	48.278	56.892
29	14.256	15.574	17.708	19.768	22.475	24.577	28.336	32.461	35.139	39.087	42.557	46.693	49.588	58.302
30	14.953	16.306	18.493	20.599	23.364	25.508	29.336	33.530	36.250	40.256	43.773	47.962	50.892	59.703

$$\underline{\underline{C}} = \frac{1}{M} \sum_{m=1}^{M} [\underline{a}(t_m) - \underline{\mu}][\underline{a}(t_m) - \underline{\mu}]^T. \qquad (28)$$

The corresponding N-dimensional Gaussian pdf is

$$p(\underline{a}) = [(2\pi)^{N/2} |\underline{\underline{C}}|^{1/2}]^{-1} \exp[-\tfrac{1}{2} (\underline{a}^T - \underline{\mu}^T)\underline{\underline{C}}^{-1}(\underline{a} - \underline{\mu})]. \qquad (29)$$

To generalize the chi-square test, we divide the observation space into I volume elements or bins, such that there are at least ten data samples in each bin. The bins do not necessarily have to be the same size. Integrating $p(\underline{a})$ over the i^{th} volume element results in a probability p_i that a data sample will fall within the i^{th} bin, if the data is jointly Gaussian. For M data points, we expect Mp_i points to fall within the i^{th} bin if $\underline{a}$ is jointly Gaussian. In fact, ν_i data points are actually observed to fall within the i^{th} bin, where the bins have been constructed such that $\nu_i > 10$.

From this point on, the chi-square test is identical to (25-26). Instead of using the number of samples that fall within an interval on the real line for a_1, we use the number of samples that fall within an N-dimensional volume element for the 1 x N vector $\underline{a}$. A multivariate Gaussian pdf replaces the univariate one as a reference function for comparison.

4.3 What if the Data Vector is Not Gaussian?

In the vicinity of a source of energy that is exciting internal waves, the natural I. W. environment may give rise to a non-Gaussian data vector [15-17]. If the chi-square test indicates that this is the

case, then it becomes necessary to estimate the multivariate distribution p(data $|H_0$). Estimates of mean and covariance are insufficient to specify a non-Gaussian p.d.f., and other methods must be used.

Although the data may be non-Gaussian due to nonlinear energy transfer phenomena [15-17], it is still reasonable to assume that the data is stationary if the energy source is stationary. For wind-surface or current-seamount excitation, a constant wind or current can be modelled as a statistically stationary source that drives a nonlinear, time-invariant filter. The output of this filter is the I.W. data at a particular position relative to the source. If the current or wind is a stationary process, then so is the internal wave data at a fixed location. Locations close to the energy source may yield non-Gaussian time series, whereas measurements taken away from the source should become Gaussian [15].

Assuming that the data is stationary, the observation space can be divided into volume elements or bins, and estimates can be made of the relative frequency of occurrence of data samples within each element. Having obtained such a histrogram, it is tempting to eliminate discontinuities by smoothing or interpolating between histogram values. For univariate probability distributions, Parzen [7] has modelled the smoothed histrogram estimate in terms of a window function that is convolved with a sample distribution. The sample distribution is just a sequence of delta functions scattered over the observation space, where each delta function represents a measured data point. Meisel [8] has discussed a multivariate version of Parzen's estimate. An example of this method, using a Gaussian window function, is given in the following paragraphs.

Let $\underline{r}$ denote the random data vector, and let $\underline{a}_m$ be the m^{th} sample vector or measurement of $\underline{r}$. It is convenient to use a symmetric, separable window function

$$W(\underline{r}) = \prod_{n=1}^{N} w(r_n) \tag{30}$$

where r_n is the random data from the n^{th} sensor, representing the n^{th} component of the observation space.

To use such a window function, the data should be normalized by making the sample variances of all observation space components equal. The measured data is

$$\{\underline{a}_m\}_{m=1}^{M} = \{[a_{m1}, a_{m2}, \ldots, a_{mN}]^T\}_{m=1}^{M} \tag{31}$$

where a_{mn} is the n^{th} component of the m^{th} data measurement. The sample variance along the n^{th} coordinate is

$$\sigma_n^2 = \frac{1}{M} \sum_{m=1}^{M} \left[a_{mn} - \frac{1}{M} \sum_{i=1}^{M} a_{in} \right]^2 . \tag{32}$$

To normalize the data, all measurements from the n^{th} sensor are divided by σ_n.

For a Gaussian window function $w(r_n)$ with window width σ, an estimate of the multivariate pdf $p(\underline{r}|H_0)$ is

$$\hat{p}(\underline{r}|H_0) = \left(\frac{1}{M}\right) \sum_{m=1}^{M} \prod_{n=1}^{N} w(r_n - a_{mn}/\sigma_n) \tag{33}$$

$$= [M(2\pi\sigma^2)^{N/2}]^{-1} \sum_{m=1}^{M} \exp\left\{ - \sum_{n=1}^{N} [r_n - a_{mn}/\sigma_n]^2 / 2\sigma^2 \right\}.$$

The choice of window width, σ, is affected by several considerations. A wide window means that many sample points are averaged in order to obtain $\hat{p}(\underline{r}|H_0)$ at any given point. From the viewpoint of robustness, this averaging would seem to be desirable. The averaging introduced by a wide window will decrease the sensitivity of the pdf estimate to the removal of any one data point, and will thereby increase the robustness of the estimate.

This reasoning suggests that we can allow the window size to become smaller as the number of observations M is increased. The motivation for making the window smaller as the data set is made larger follows from Parzen's condition for an unbiased pdf estimate [7]. This condition implies that estimates of the form (33), where w(r) is Gaussian with standard deviation $\sigma(M)$ are asymptotically unbiased if

$$\lim_{M \to \infty} \sigma(M) = 0. \tag{34}$$

The above condition, together with the condition [7]

$$\lim_{M \to \infty} M\sigma(M) = \infty \tag{35}$$

assures that the variance of the pdf estimate approaches zero for a continuous pdf, as $M \to \infty$. In summary, (34-35) are Parzen's conditions for unbiased and consistent pdf estimates. They state that the window size should become small as M becomes large, but not so small as to violate (35). For any finite M, the Parzen pdf estimates are biased [7].

4.4 What if the Data Vector is Gaussian?

If internal waves away from an energy source result in stationary, Gaussian-distributed measurements in the absence of an unusual disturbance, then an unusual disturbance can be detected because it destroys the stationarity of the data. Haubrich [18] has devised a test for stationarity that is based on the fact that stationary processes have uncorrelated spectral coefficients [11]. In order to distinguish between correlated and uncorrelated coefficients, Haubrich has measured the coherence between coefficients and has compared the pdf of this measurement with the pdf that is expected for a Gaussian, stationary process.

There are two basic flaws in Haubrich's approach. First, his paper presents no independent test for joint Gaussianity of his observations. Thus, if the probability distribution of the coherence estimate differs from the pdf corresponding to a stationary, Gaussian I.W. process, it is unclear whether this difference is caused by lack of stationarity or lack of Gaussianity. The same criticism applies to bispectral analysis [28-34]. A nonzero bispectrum may be caused by either nonlinear interactions (which result in non-Gaussianity) or by non-stationarity. This defect is remedied by using a multivariate chi-square test for joint Gaussianity, as in Section 4.2.2. If the data is Gaussian, then nonzero coherence or bispectra must be caused by nonstationarity.

The second flaw in Haubrich's paper is that differences in distributions are identified by using histograms of "outliers," i.e., points that fall at the extremes of the observation range. This problem is easily corrected by again using a chi-square test,

where the reference distribution corresponds to the distribution of the coherence estimate for stationary, Gaussian data [18-20].

5.0 INTERNAL WAVE MEASUREMENTS WITH DOPPLER SONAR

5.1 Present Method

An ingenious method for remote sensing of internal waves has been conceived and implemented by Pinkel [21]. Using ultrasonic echoes from small volume scatterers, Pinkel can determine the mean velocity of water in a range-Doppler resolution cell. The resulting plots of mean echo frequency as a function of range and time illustrate the velocity perturbations that are caused by internal waves, and provide data for construction of a frequency-wave number spectrum.

In order to simplify the signal processor, the Doppler sonar presently uses the echo covariance function to estimate the first moment of the echo power spectrum [21, 22]. The concept of a power spectrum implies stationarity, whereas we actually expect the center frequency to change with time as the wave moves through a given resolution cell. The process is thus based on a local stationarity assumption [12]; it is assumed that measurements can be taken over a temporal and spatial interval that is small enough to avoid nonstationarity effects. The use of a first moment measure also implicitly assumes that water motion is nearly uniform within the resolution cell of the sonar, or at least that the spectral distribution of the echo is not multimodal.

The autocovariance function of the echo e(t) is

$$R_{ee}(\text{time, range}) = R_{ee}(\tau, D) \equiv R_{ee}(\tau) \qquad (36)$$

within any one range resolution cell. The echo e(t) has an analytic representation

$$e(t) = x(t) + j\,y(t) \tag{37}$$

where y(t) is the Hilbert transform of x(t). For any transmitted signal, a sample of x(t) is obtained by delaying the signal by 2D/c, multiplying the echo data by the signal, and integrating over the duration of the signal. A sample of y(t) is obtained by multiplying echo data by the Hilbert transform of the signal and integrating. For sinusoidal signals, x(t) and y(t) can be obtained by quadrature demodulation.

The mean frequency is

$$\bar{f} = \frac{\int_0^\infty f\, S_{ee}(f)\, df}{\int_0^\infty S_{ee}(f)\, df}$$

$$= \frac{\frac{d}{d\tau} R_{ee}(\tau)\Big|_{\tau=0}}{2\pi j\, R_{ee}(0)} = \frac{\dot{R}_{ee}(0)}{2\pi j\, R_{ee}(0)}. \tag{38}$$

From (37)

$$R_{ee}(\tau) = A_e(\tau) \exp\left[j\, 2\pi\, \phi_e(\tau)\right]$$

where $A_e(\tau)$ is an even function of τ and $\phi_e(\tau)$ is an odd function of τ, since $S_{ee}(\tau)$ is real. It follows that

$$\bar{f} = \frac{1}{2\pi j} \frac{\dot{R}_{ee}(0)}{R_{ee}(0)} = \dot{\phi}_e(0). \tag{39}$$

It is easy to compute $R_{ee}(0)$ and $R_{ee}(\Delta)$ for a single delay Δ. Then

$$\bar{f} = \dot{\phi}_e(0) \approx \frac{\phi_e(\Delta) - \phi_e(0)}{\Delta} = \frac{\phi_e(\Delta)}{\Delta}$$

$$= \frac{1}{\Delta} \operatorname{Arctan} \frac{\operatorname{Im}\{R_{ee}(\Delta)\}}{\operatorname{Re}\{R_{ee}(\Delta)\}}. \tag{40}$$

Miller and Rochwarger [22] have pointed out that the variance of the power spectrum can also be estimated from two covariance samples. The mean-square width of the spectrum about its mean is

$$\bar{\sigma}^2 = \frac{\int f^2 S_{ee}(f)\, df}{\int S_{ee}(f) df} - \bar{f}^2$$

$$= -\frac{1}{(2\pi)^2} \left\{ \frac{\ddot{R}_{ee}(0)}{R_{ee}(0)} - \left[\frac{\dot{R}_{ee}(0)}{R_{ee}(0)}\right]^2 \right\}$$

$$= \frac{1}{(2\pi)^2} \frac{\ddot{A}_e(0)}{A_e(0)}$$

$$\approx -\frac{1}{4\pi^2 A_e(0)} \left[\frac{A_e(\Delta) + A_e(-\Delta) - 2A_e(0)}{\Delta^2}\right]$$

$$= \frac{1}{2\pi^2\Delta^2} \left[1 - \frac{A_e(\Delta)}{A_e(0)}\right];$$

$$\bar{\sigma} = \frac{1}{\sqrt{2}\pi\Delta}\left[1 - \frac{|R_{ee}(\Delta)|}{|R_{ee}(0)|}\right]^{\frac{1}{2}}. \qquad (41)$$

Both the mean frequency and the rms bandwidth of the echo e(t) can be determined from

$$R_{ee}(0) = E\{|e(t)|^2\} \qquad (42)$$

and

$$R_{ee}(\Delta) = E\{e(t)\,e^*(t+\Delta)\}, \qquad (43)$$

i.e., from the echo cross-correlation function at a single delay Δ (e.g., the spacing between successive transmitted pulses) and the average power in the echo. It would appear that $\bar{\sigma}$ is not calculated in the existing Doppler sonar system.

5.2 Possible Problems and Improvements

5.2.1 Spatial Sampling

The 1° beamwidth of the sonar system at 75 KHz means that the beam diameter exceeds 10m at ranges greater than 600 m. Recall that 10m was our minimum sample spacing, obtained from the sampling theorem. A 10 meter-wide beam is not the same as a 10 meter sampling interval, since spatial averaging occurs across the beam. Nevertheless, a beam can be modelled as a spatial impulse response function that is convolved with the data. The corresponding low-pass spatial filter has a cut-off frequency

of $\pm 0.05\ m^{-1}$ for a 10 m wide beam, and this passband should be sufficiently wide for the data of interest, as in (6).

Pinkel has reported a range resolution of approximately 25 m for his system. Samples that are 25 m apart are theoretically too far apart for unique reconstruction of the environment. To assess the practical significance of such a large resolution cell, one can try to see whether Doppler shifts sometimes experience a drastic change within a single range bin. For example, a very high wave number internal wave with a 20 m wavelength will exhibit a large range of velocities within a 25 meter interval.

The present implementation of the Doppler sonar assumes that no appreciable velocity changes occur over a 30 m interval, on the basis of a coherence argument [21]. Having made this assumption, only the first moment of the echo power spectrum is measured. This measurement method results in a self-fulfilling prophecy; having assumed that there is no Doppler spreading or multimodal spectrum, we do not see any.

In order to check on the sufficiency of a 25 m resolution cell, it is necessary to refine the Doppler processor or to compare identical data that is measured with 25 m and 10 m range resolutions.

To refine the Doppler processor, one can measure the width of the echo spectrum by using (41). This width, however, may not be very indicative of multiple velocities from a high-wavenumber event, since the relatively large velocities and amplitudes of low frequency-wavenumber events will probably dominate the spectrum. It is desirable to look at the whole Doppler

spectrum from a number of 25 m range intervals, and to decide whether such spectra may be multimodal or spread due to high frequency-wavenumber events. It should be possible to perform this analysis from tape-recorded echo data.

Another approach is to measure the same data with both 25 m and 10 m resolution cells. Better range resolution can be obtained by using a broader transmitted bandwidth. Bandwidth can be broadened without degrading the velocity estimate if coding or modulation is used, i.e., if the signal has large time-bandwidth product.

Another way to improve the range resolution is simply to use a time gate that isolates a 10 m echo interval for each transmitted pulse. If all the scatterers in the 10 m interval are moving uniformly, then they will experience a range displacement equal to

$$\delta = 2(v \cos \theta)\Delta \tag{44}$$

between two signals that are Δ seconds apart, where $v \cos \theta$ is the radial velocity component of the scatterers. For a transmitted frequency f_0, this displacement results in a phase change

$$\phi = 2(v \cos \theta)\, \Delta\, (2\pi f_0/c). \tag{45}$$

A sequence of pulses thus results in a sequence of phase shifts, which show up as a frequency shift

$$f_d = 2(v \cos \theta)\, f_0/c \tag{46}$$

when the echoes are Fourier transformed. The accuracy of the f_d estimate depends upon the length of the time integral for calculating

the Fourier transform, which is proportional to the number of gated echoes that are coherently processed.

In terms of spectral moment estimation, the gated echoes $\{e_n(t)\}_{n=1}^{N}$ for N transmitted pulses with pulse repetition interval Δ are used to compute

$$R(0) = \sum_{n=1}^{N} |e_n(t)|^2 \tag{47}$$

$$R(\Delta) = \sum_{n-1}^{N-1} e_n(t)\, e^*_{n+1}(t). \tag{48}$$

It is not necessary to store all the pulses at the same time, since

$$R(0) = R_N(0) \tag{49}$$

$$R(\Delta) = R_N(\Delta) \tag{50}$$

where

$$R_n(0) = R_{n-1}(0) + |e_n(t)|^2 \tag{51}$$

$$R_n(\Delta) = R_{n-1}(\Delta) + e^*_n(t)\, e_{n-1}(t). \tag{52}$$

Thus, only $e_n(t)$ and $e_{n-1}(t)$ need to be stored at any given time. Similarly, the Fourier integral or discrete Fourier transform can be divided into a superposition of integrals or sums over disjoint time intervals, and this superposition can be calculated recursively.

In summary, the spatial sampling that is presently used by the Doppler sonar may be too coarse. Resolution can be improved by limiting range to less than 600 m and by using a narrow range

gate with pulse-to-pulse coherent processing, which can be implemented recursively.

5.2.2 Increasing the Accuracy of I.W. Velocity Estimates

5.2.2.1 Resolution Limits

Internal waves with high frequencies and wavenumbers tend to propagate very slowly. For a two-minute processing time, velocity resolution can theoretically be as fine as 1/120 cm/sec for a 75 KHz center frequency, i.e.,

$$2 f_0 \Delta v/c = 1/T$$

and

$$\Delta v = \frac{c}{2 f_0 T} = \frac{150,000 \text{ cm/s}}{150,000\ T} = \frac{1}{T} \text{ cm/sec.} \qquad (53)$$

The above limit applies for an optimum (matched filter) velocity estimator.

According to Pinkel, such fine velocity resolution could be wasted, since random motion of the scatterers will result in a minimum echo spectral width of $1/\tau_c$, where τ_c is the scattering correlation time. It would seem, however, that the effects of random scatterer motion, along with uniform migration of scatterers, can be significantly reduced by spatial filtering.

5.2.2.2 Spatial Filtering

Spatial filtering represents a post-processing method that can be used to improve high resolution Doppler data. The method is based on the observation that the spatial frequency spectrum of scatterer motion in the absence of an internal wave is usually different from the I.W. spectrum. Uniform migration of scatterers will result in a Doppler shift that is nearly constant from one resolution cell to the next, and the corresponding spatial frequency is near zero. Random motion of scatterers will usually be decorrelated from one resolution cell to the next, resulting in a uniform distribution of spatial frequencies. A spatial filter that passes only the I.W. spectrum of interest (e.g., high wavenumber events) should then be capable of eliminating much of the scatterer motion that is unrelated to the presence of an internal wave.

5.2.2.3 Optimum Signal Processing

The main reason for the use of covariance derivatives to generate spectral moments is the simplicity of the resulting sonar signal processor [21]. Optimum signal processing involves the use of matched filters, which can become quite complicated when large time-bandwidth signals are used [23]. In the near future, however, fast Fourier transforms will become available as large-scale integrated circuits, and a Fourier transformer will be just another off-the-shelf logic component, like a shift register, adder, or accumulator. Already, integrated circuits exist for performing many of the operations in a pipeline FFT [24]. The availability of near-real-time, easy-to-implement Fourier transformers will greatly affect the feasibility of optimum signal processing techniques

for I. W. Doppler sonar. The connection between Fourier transforms and velocity sensing is discussed in [25, 26]. The main points of this discussion are summarized below.

The Doppler shifts of many different moving scatterers at various ranges can be summarized in terms of a scattering function, $\Gamma(t, f)$. The scattering function describes the Doppler shifts that are introduced by the medium as a function of range. The scattering function can be measured by forming a time window spectrogram of the echo data, e(t).

The spectrogram is formed by multiplying the echo by a delayed window function $w(t - \tau)$ and computing the Fourier transform of the product:

$$S_{ew}(\tau, \phi) \equiv \left| \int_{-\infty}^{\infty} e(t)\, w(t-\tau)\, \exp(-j2\pi\phi t)\, dt \right|^2. \tag{54}$$

Let w(t) be a time-reversed version of v(t), i.e.,

$$v(t) = w(-t). \tag{55}$$

Then [25]

$$E\{S_{ev}(\tau, \phi)\} \equiv \Gamma(t, f) \overset{t,f}{*} S_{uv}(t, f) \tag{56}$$

where u(t) is the transmitted sonar signal and $\overset{t,f}{*}$ denotes two-dimensional convolution. In (56), $\Gamma(t, f)$ is the scattering function, which we would like to measure, and $S_{uv}(t, f)$ is the spectrogram of the transmitted signal. $E\{\cdot\}$ denotes ensemble average.

Eq. (56) says that the echo spectrogram is a smeared version of the scattering function, where the smearing is caused by convolution with the spectrogram of the input signal. To reduce the smearing effect, the input signal u(t) and the window function w(t) should be designed to produce a thumbtack-like signal spectrogram, $S_{uv}(t, f)$.

The problem of choosing an appropriate signal u(t) and window function w(t) = v(-t) reduces to a standard signal design problem by virtue of the fact that [25]

$$S_{uv}(\tau, \phi) = |\chi_{uw*}(-\tau, \phi)|^2, \tag{57}$$

where $\chi_{uw*}(-\tau, \phi)$ is the cross-ambiguity function of the signal and window functions.

For a narrowband echo, an optimum estimate of center frequency that is obtained from spectrogram observations has an rms error σ_d such that

$$\sigma_d \sim [T_u T_w]^{-\frac{1}{2}}, \qquad T_w \leq T_u \tag{58}$$

[25], where T_u is the signal duration and T_w is the window duration. The rms error is minimized when the window and signal have the same duration, e.g., when the window is matched to the signal. In this case, $w(t) = u^*(t)$, and

$$E\{S_{ev}(\tau, \phi)\} = \Gamma(t, f) \overset{t, f}{*} |\chi_{uu}(-t, f)|^2, \tag{59}$$

where

$$|\chi_{uu}(-\tau, \phi)|^2 \equiv \left| \int_{-\infty}^{\infty} u(t)\, u^*(t-\tau) \exp(-j2\pi\phi t)\, dt \right|^2 \tag{60}$$

and $S_{ev}(\tau, \phi)$ is given by (54-55).

From (54), we see that optimum, matched-filter processing to estimate the scattering function of the ocean (and hence to extract Doppler variations that are induced by internal waves) is accomplished by multiplying echo data by an appropriate window function and by Fourier transforming the resulting product. This process should become easier to implement as LSI FFT circuits become available, or through the use of array processors [27] or pipeline hardware FFT algorithms [24].

5.2.2.4 Signal Design

If matched filtering or window multiplication/FFT processing is employed, then it is desirable to find signals that have better than 10 m range resolution and sufficient Doppler resolution for mapping the slowest internal waves (i.e., those with high frequencies and wave numbers). For a 7.5 m range resolution, the signal bandwidth should be [23]

$$B = \frac{c}{2\Delta R} = 100 \text{ Hz.} \tag{61}$$

For a 0.5 cm/s velocity resolution, the signal duration for $f_0 = 75$ KHz should be [23]

$$T = \frac{c}{2 f_0 \Delta v} = 20 \text{ sec.} \tag{62}$$

The required time-bandwidth product is then 2000. If a coded waveform is used, then each pulse in the code should have a duration of .01 sec, and 2000 such pulses are needed. Two thousand numbers must be stored (e.g., in a read-only memory) in order to generate the signal and the window function or reference waveform.

The signal should be designed to produce an ideal, thumbtack-like ambiguity function [23]. Alternatively, one can exploit the fact that the expected Doppler shifts are limited, and the signal can be designed such that $|\chi_{uu}(\tau, \phi)|^2 = 0$ for [1/20 Hz] < $|\phi|$ < the maximum expected Doppler shift, ϕ_{max}. A region of the ambiguity plane would thus be free of ambiguity volume, producing a "volume-free area" [23]. For example, one could transmit a sum of twenty-second-long sinusoids with random center frequencies, provided that the minimum spacing between frequencies is greater than the maximum possible Doppler shift, as in Figure 1. The autocorrelation function of the signal is the inverse Fourier transform of the power spectrum. The use of irregularly spaced center frequencies should decrease the sidelobe level of the autocorrelation function, which would be quite large for uniformly spaced sinusoids.

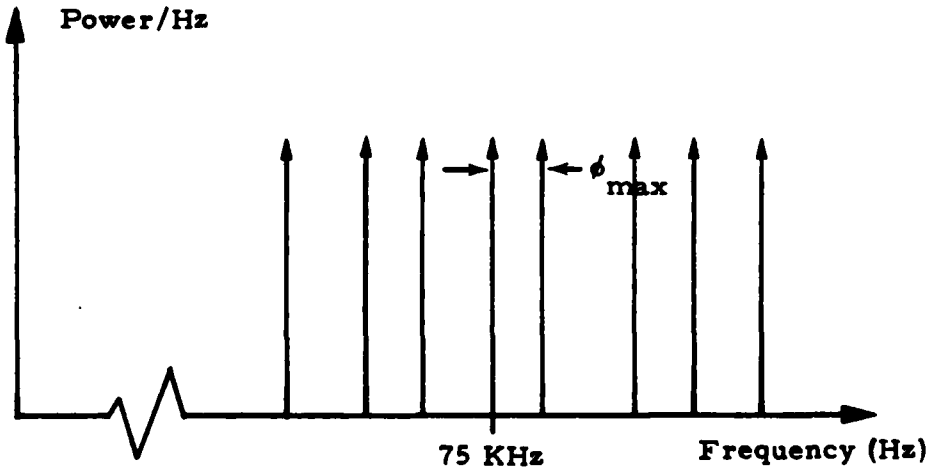

Figure 1. Power spectrum of a signal designed for volume-free-area for Doppler shifts between 1/20 Hz and ϕ_{max}.

5.2.3 Identification of Sidelobe Returns

Pinkel has pointed out that a major source of error may be echoes from scatterers that are not in the main beam, i.e., echoes that enter the receiver through sidelobes of the beam. Doppler measurements at two different frequencies may help to resolve this difficulty.

If an array of N transducer elements in the x-y plane is excited by a sinusoid at frequency f, the received signal at a point in the far field that is θ_x radians off boresight in the x direction is

$$A(\theta_x, f) = \sum_{n=1}^{N} \exp\left[-j2\pi f(R - x_n \sin\theta_x)/c\right] \tag{63}$$

where R is the distance from the observation point to the center of the array, and x_n is the x-component of the position of the n^{th} element, relative to the array center. If θ_x is less than $\pi/6$, then $\sin\theta_x \approx \theta_x$, and

$$\begin{aligned} |A(\theta_x, f)|^2 &= \left| \sum_{n=1}^{N} \exp\left[j(2\pi f x_n \sin\theta_x)/c\right] \right|^2 \\ &\approx \left| \sum_{n=1}^{N} \exp\left[j2\pi x_n (f\theta_x)/c\right] \right|^2 \\ &= |A(f\theta_x)|^2. \end{aligned} \tag{64}$$

The radiation pattern of the array is thus scaled when f changes. The effect of the scaling becomes larger for large angles away from zero (boresight). Near boresight, a frequency change has

little effect. At points that are removed from boresight, the radiation pattern can change considerably.

We would like to know the contribution of scatterers that are off-boresight to the measured echo. This contribution can be assessed by comparing I. W. echoes that are measured at nearly the same time, but at two different frequencies. A basic test is to cross correlate frequency translated, "raw" echo data. The echo at a given frequency is translated to baseband, using the transmitted frequency as a local oscillator signal. The echo at a different frequency, measured at nearly the same time, is processed in the same way. The two baseband echoes are random processes that are induced by scattering of a sinusoid from many randomly-distributed point targets. If the same "cloud" of point targets gives rise to both echoes, the two baseband returns will be highly correlated. If, however, different random point targets are illuminated, then there should be very little correlation between the two baseband echoes.

Sidelobes that are away from boresight will move to new angles when frequency is changed, and they will illuminate different scatterers than before. The resulting baseband echoes will be decorrelated at the two frequencies. For signal energy at boresight, there will be little change in the illuminated scatterers when frequency changes, and baseband echoes from scatterers near boresight will be highly correlated at the two transmitted frequencies.

The correlation coefficient between baseband echoes obtained at different transmitted frequencies is then a measure of sidelobe contributions. A correlation coefficient that is near unity indicates relatively small contributions from sidelobes.

To identify Doppler echoes from sidelobes, one can again use the baseband echoes that are derived from two different transmitted frequencies. The power spectra of the two echoes should be different for echo components that are received through sidelobes. This difference should occur because of a re-orientation of the sidelobe positions when frequency is changed, in accordance with (64). A different angle between a sidelobe and the velocity vector results in a different Doppler shift. Observed spectral differences in baseband echoes can be used to construct a weighting function for spectral conditioning. Those Doppler frequencies that exhibit little amplitude change are given larger weights than Doppler shifts that exhibit large spectral amplitude change when the transmitted frequency is changed. The resulting spectral weighting function may turn out to be asymmetric, which would indicate that unweighted estimates of average Doppler shift are biased.

5.2.4 Multiple Beams

In Section 3, the concepts of homogeneity, isotropy, and separability were discussed. Homogeneity implies that spatial autocovariance functions depend only upon spatial shifts and not upon the location at which measurements are obtained. The shift dependence, however, can vary with direction of shift. Isotropy implies that shift dependence is not direction dependent; the same spatial autocovariance function is measured no matter what the shift direction. Separability means that the autocovariance function $R(\Delta x, \Delta y, \Delta z)$ can be written as a product $R_x(\Delta x)\, R_y(\Delta y)\, R_z(\Delta z)$.

Physically, homogeneity is expected when wave propagation occurs in a homogeneous medium, without physical boundaries or

other spatial variations. In the ocean, this condition does not hold in the vertical direction, but should hold in the horizontal plane at any given depth. Autocovariance functions and frequency-wavenumber spectra must then be indexed by a depth variable:

$$R(\Delta x, \Delta y, z, \Delta t) \equiv E\{a(x, y, z, t)\, A^{*}(x+\Delta x,\ y+\Delta y,\ z,\ t+\Delta t)\}$$

and

$$\iiint R(\Delta x, \Delta y, z, \Delta t)\, e^{-j(k_x \Delta x + k_y \Delta y + \omega \Delta t)}\, d(\Delta x)\, d(\Delta y)\, d(\Delta t)$$

$$= S_z(k_x,\ k_y,\ \omega).$$

Isotropy is expected when there is no preferred direction of internal wave propagation. This condition should occur in a horizontal plane in deep water, away from continental disturbances, and away from energy sources that create internal waves, such as seamounts. If a random field is isotropic as well as homogeneous, then it is only necessary to measure the autocovariance function shifts in one direction, since shifts in all other directions will give the same result. Thus, $R(\Delta x,\ z,\ \Delta t)$ completely describes autocovariance behavior, and

$$\iint R(\Delta x, z, \Delta t)\, e^{-j(k_x \Delta x + \omega \Delta t)}\, d(\Delta x)\, d(\Delta t)$$

$$= S_z(k_x,\ \omega)$$

is a complete description of the spectrum in a horizontal plane at depth z.

Although isotropy can often be assumed for characterization of the natural I. W. environment, it is not a good assumption

if the same system is to be used for detecting unnatural disturbances, such as wakes.

Separability is expected when there is reason to believe that the autocovariance function will be symmetric about the x and y axes. Symmetry follows from the fact that, if

$$R(\Delta x, \Delta y, z, \Delta t) = R_x(\Delta x, 0, z, \Delta t)\, R_y(0, \Delta y, z, \Delta t)$$

then $|R_x(\Delta x, 0, z, \Delta t)|$ should be a symmetric function of Δx, in order that the power spectrum be real. Similarly, $|R_y(0, \Delta y, z, \Delta t)|$ is expected to be a symmetric function of Δy, for any given value of Δx.

On the basis of the above concepts, some observations can be made about the suitability of various beam patterns for Doppler sonar IW investigations:

1. A vertical beam can be used to assess the degree of spatial inhomogeneity that exists for internal waves.

2. An isotropic assumption would allow data in a horizontal plane to be gathered with a single beam. At any given time, observed internal wave packets will probably be non-isotropic. Isotropy is expected only for large ensemble averages of IW wave measurements. It takes a whole day for a wave that moves at 1 cm/s to travel about 1 km. To gather enough data for isotropy to hold, one must either wait for many days, or transport the sonar to a new location.

3. If two orthogonal horizontal beams are used, then a separability assumption is being invoked in order to

reconstruct a frequency-wavenumber spectrum. Again, it is doubtful that such an assumption holds for individual wave packets, and it is necessary to ensemble average measurements that are taken at different locations or on different days.

4. If tilted horizontal beams are used, then the data from different depths must be processed separately, because of vertical inhomogeneity. A beam that is depressed 45° down for example, investigates only a 30 m variation in Δx, Δy for each 30-m thick horizontal layer. Presumably, $R(\Delta x, \Delta y, z, \Delta t)$ should be calculated for Δx and Δy greater than 30 meters. A more shallow depression angle is then needed, unless vertical homogeneity holds over more than 30 m. An alternative is to use many different depression angles, which would allow the sonar to gather data from different locations in a horizontal plane at each depth. Such vertical scanning, however, may be difficult to implement with the present system.

6.0 SUMMARY AND CONCLUSION

Internal wave characterization has been conceived as the specification of a multivariate probability density function. The number of variables in this function is determined by the sampling theorem, which also indicates maximum sensor spacing.

Stationarity assumptions in time and space have been discussed, and spatial stationarity has been considered in the form of homogeneity and isotropy.

Autocovariance functions and frequency-wavenumber spectra are especially meaningful if the data is Gaussian, as well as stationary. A test for multivariate joint Gaussianity has been introduced. If the data is not sufficiently Gaussian, one can resort to estimation of the probability distribution using a Parzen window.

Doppler sonar for IW measurements has been discussed, and possible improvements have been presented. An important aspect of this discussion is the concept that a Doppler sonar should ideally try to measure a scattering function, and that this measurement is best accomplished by using Fourier analysis rather than spectral moment estimation. Even with the present system, post-processing data with a spatial filtering operation should help to eliminate the effects of noise, random scatterer motion, and scatterer migration.

If a Fourier analysis capability is built into the system, then ROM-generated window functions can be used to implement an ideal sonar processor, with better resolution and SNR than can presently be obtained.

Finally, the use of multiple beams in a Doppler sonar has been discussed in the context of stationarity, homogeneity, and separability of the random field of internal wave measurements. Homogeneity and separability assumptions are likely to hold only for large ensemble averages. Such averages may suppress non-stationary events such as man-made wakes. Estimation of $p(\text{data}|H_0)$ is thus much different from estimation of $p(\text{data}|H_1)$. It is also likely that the observed background for any given man-made event will not be accurately described by $p(\text{data}|H_0)$ unless the data is observed over several days.

7.0 REFERENCES

1. H. L. Van Trees, Detection, Estimation, and Modulation Theory, Part I. New York, Wiley, 1968.

2. C. E. Shannon and W. Weaver, The Mathematical Theory of Communication. Urbana, Univ. of Illinois, 1964.

3. C. Garrett and W. Munk, "Space-time scales of internal waves," Geophys. Fluid Dyn. 2, 225-264, 1972.

4. E. J. Katz, "Tow spectra from MODE," J. Geophys. Res. 80, 1163-1167, 1975.

5. R. Pinkel, "Upper ocean internal wave observations from Flip," J. Geophys. Res. 80, 3892-3910, 1975.

6. K. D. Leaman and T. B. Sanford, "Vertical energy propagation of internal waves," J. Geophys. Res. 80, 1975-1978, 1975.

7. E. Parzen, "On estimation of a probability density function and mode," Ann. Math. Stat., Vol. 33, Part 2, 1065-1076, 1962.

8. W. S. Meisel, Computer-Oriented Approaches to Pattern Recognition. New York, Academic, 1972.

9. E. T. Jaynes, "Information theory and statistical mecahnics, Part I," Phys. Rev. 106, 620, 1957.

10. E. T. Jaynes, "Information theory and statistical mechanics, Part II," Phys. Rev. 108, 171, 1957.

11. A. M. Yaglom, Stationary Random Functions. Englewood Cliffs, Prentice-Hall, 1962.

12. R. A. Silverman, "Locally stationary random processes," IRE Trans. Inform. Theory, IT-3, 182-187, 1957.

13. H. Cramér, Mathematical Methods of Statistics. Princeton, Princeton Univ. Press, 1946.

14. R. A. Fisher, Statistical Methods for Research Workers. Eighth ed., Edinburgh, Oliver and Boyd, 1941.

15. C. H. McComas, "Equlibrium mechanisms within the oceanic internal wave field," J. Phys. Oceanography, Vol. 7, 836-845, 1977.

16. M. G. Briscoe, "Gaussianity of internal waves," J. Geophys. Res. 82, 2117-2126, 1977.

17. C. Wunsch, "Deep ocean internal waves: what do we really know?," J. Geophys. Res. 80, 339-343, 1975.

18. R. A. Haubrich, "Earth noise, 1. Spectral stationarity, normality, and nonlinearity," J. Geophys. Res. 70, 1415-1427, 1965.

19. W. R. Goodman, "Measurement of matrix frequency response functions and multiple coherence functions," Air Force Flight Dynamics Laboratory, Wright-Patterson AFB, Ohio, Report AFFDL-TR-65-56, June 1965.

20. G. C. Carter, "Estimation of the magnitude-squared coherence function," AD 743 945, 1972.

21. R. Pinkel, "On the use of Doppler sonar for internal wave measurements," Report MPL-U-63/79, Scripps Inst. of Oceanography, 1979.

22. K. S. Miller and M. M. Rochwarger, "A covariance approach to spectral moment estimation," IEEE Trans. Inform. Theory, Vol. IT-18, 588-596, 1972.

23. C. E. Cook and M. Bernfeld, Radar Signals. New York, Academic, 1967.

24. H. L. Groginsky and G. A. Works, "A pipeline fast Fourier transform," IEEE Trans. Comput., C-19, 1015-1019, 1970.

25. R. A. Altes, "Detection, estimation, and classification with spectrograms," J. Acous. Soc. Am. 67, 1232-1246, 1980.

26. R. A. Altes and W. J. Faust, "A unified method of broadband echo characterization for diagnostic ultrasound," to appear in IEEE Trans. on Engineering in Medicine and Biology.

27. G. D. Bergland, "Fast Fourier transform hardware implementations -- an overview," IEEE Trans. Audio Electroacoust., AU-17, 104-108, 1969.

28. K. Hasselmann, W. Munk, and G. MacDonald, "Bispectra of ocean waves," in Time Series Analysis, M. Rosenblatt, ed., Wiley, N. Y., 1962, pp. 125-139.

29. N.-C. Yao, S. Neshyba, and H. Crew, "Rotary cross-bispectra and energy transfer functions between non-Gaussian vector processes," J. Phys. Ocean., Vol. 5, 1975, pp. 164-172.

30. S. Neshyba and E. J. C. Sobey, "Vertical cross coherence and cross bispectra between internal waves measured in a multiple-layered ocean," J. Geophys. Res., Vol. 80, 1975, pp. 1152-1162.

31. D. J. Bendiner and G. I. Roden, "Bispectra and cross-bispectra of temperature, salinity, sound velocity, and density fluctuations with depth off northeastern Japan," J. Phys. Oceanog., Vol. 3, 1973, pp. 308-317.

32. J. W. Tukey, "What can data analysis and statistics offer today?," in Ocean Wave Spectra, National Academy of Sciences and U.S. Naval Oceanographic Office, Easton, Md., 1961, pp. 347-351.

33. M. Rosenblatt and J. W. Van Ness, "Estimation of the bispectrum," Ann. Math. Stat., Vol. 36, 1965, pp. 1120-1136.

34. J. W. Van Ness, "Asymptotic normality of bispectral estimates," Ann. Math. Stat., Vol. 37, 1966, pp. 1257-1272.

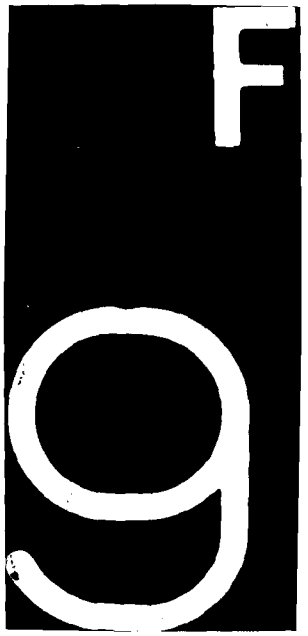
F
9